4.3.2 Meteors

INGRID MANN

4.3.2.1 Introduction

4.3.2.1.1 Meteor phenomenology

Detection: Meteors are phenomena that occur on time spans of the order of milliseconds to minutes and are caused by entry of solid objects of interplanetary matter (meteoroids) into the Earth's atmosphere. Originally the term meteor describes the luminous phenomenon, i.e. the emitted visible brightness, generated upon meteoroid entry [02Haw]. This is typically observed at altitudes between 120 km and 80 km above the Earth's surface. The entry of large objects is observed downward to 20 km (i.e. fireballs, see below). Meteors are also actively detected by radar [02Bag] and passively by acoustic, infrasonic and seismic signals (summarized in [98Cep]). Remnant species in the atmosphere can be detected with the radar and LIDAR techniques [99Zah].

Entry process: Meteoroids that enter the Earth's atmosphere are heated as a result of the momentum transfer from atmospheric species. The energy transfer from this process is counter balanced by energy loss by radiation and internal processes, mostly in thermochemical transitions. Small dust particles (smaller than about 50 micrometer) efficiently reradiate the entry heat and experience only moderate temperature increase. Objects larger than a couple of 100 micrometer are heated to melting and evaporation temperatures. The meteoroid mass loss as a result of the entry is called ablation. Ablation may appear in solid fragment, fluid or gaseous form depending on the stage of the entry process. Meteoroid and atmospheric species are partly ionized and form a column (trail or train, see below) behind the meteoroid. The evolving plasma column has an initial radius of several 10 cm to several meter [98Cep] and it causes the observed phenomena.

In the initial stage in the tenuous upper atmosphere the impact of individual atmospheric species causes moderate heating of the meteoroid. Release of material from the meteoroid surface (e.g. sputtering) and surface reactions (e.g. scattering) of the impinging atmospheric species occur. The preheating stage ranges over heights of 400 to 120 km. In the denser lower atmosphere the meteoroid surface is heated to evaporation temperature and meteoroid and atmospheric species dissociate and ionize as a result of mutual collisions (ablation stage from about 120 to 80 km). This stage is associated with the typical meteor brightness. Fragmentation of the meteroid into solid fragments may also occur during this stage, but the majority of the kinetic energy of the entry transforms into vaporization of the meteoroid material. Parts of the meteoroid that survive until deceleration to less than 3 km/s continue a dark flight. The exact altitudes of the different stages of the entry process vary with velocity, mass and composition of the entering meteoroid.

Remnants: Small meteoroids, gaseous species that originate from the meteoroids, as well as meteoritic smoke particles that form by re-condensation of the gaseous component are incorporated into the atmosphere and influence its chemical and physical processes [80Hun, 02Mur, 08Meg]. Some remnants of meteoroids, i.e. meteorites or micrometeorites, reach the ground and their inner parts possibly remain without material alteration (see Section 4.3.3 "Meteorites" of this issue). The interplanetary dust particles that are collected in the upper atmosphere, as a result of their moderate entry heating, show no significant alteration. The meteor phenomenon also occurs in the atmospheres of other planets and solar system objects [07Chr].

4.3.2.1.2 Definitions

The following definitions of terms were establishd by the International Astronomical Union (IAU) Commission 22 and were published including the corresponding French, Russian, and German terms [63Mil,.They are repeated here with minor modifications and are used within this chapter]:

- A **meteor:** in particular, the light phenomenon, which results from the entry into (usually the Earth's) atmosphere of a solid particle from space; more generally, as a noun or an adjective, any physical object or phenomenon associated with such an event.
- B **meteoroid:** a solid object moving in interplanetary space, of a size considerably smaller than an asteroid and considerably larger than an atom or molecule.
- C **meteorite:** any object defined under B, which has reached the surface of the Earth without being completely vaporized.
- D **meteoric:** the adjectival form pertaining to definitions A and B.
- E **meteoritic:** the adjectival form pertaining to definition C.
- F **fireball:** a bright meteor with luminosity, which equals or exceeds that of the brightest planets (visual magnitude −4). Fireballs are also called bolides.
- G **micrometeorite:** a very small meteorite or meteoritic particle with a diameter in general less than a millimeter.
- H **dust (**when used with D or E)**:** finely divided solid matter, with particle sizes in general smaller than micrometeorites.
- I **absolute magnitude:** the stellar magnitude any meteor would have in the absence of atmospheric absorption if placed in the observer's zenith at a height of 100 km.
- K **trajectory:** the line of motion of the meteor relative to the Earth, considered in three dimensions.
- L **path:** the projection of the trajectory on the celestial sphere, as seen by the observer.
- M **train:** anything (such as light or ionization) left along the trajectory of the meteor after the head of the meteor has passed (also called ‘trail’).
- N **persistent:** adjectival form for use with M indicating durations of some appreciable time.
- O **wake:** train phenomenon of very short duration, in general much less than a second.
- P **radiant:** the point where the backward projection of the meteor trajectory intersects the celestial sphere.
- Q **earth-point:** the point where the forward, straight line projection of the meteor trajectory intersects the surface of the Earth.
- R **zenith attraction**: the effect of the Earth’s gravity on a meteoritic body increasing the velocity and moving the radiant towards the zenith.
- S **orbit:** the line of motion of a meteoric body when plotted with reference to the Sun as origin of co-ordinates.
- T **shower (**for use with A or D)**:** a number of meteors with approximately parallel trajectories.
- U **stream (**for use with A or D)**:** a group of meteoric bodies with nearly identical orbits.
- (additional definitions, not included in [63Mil])
- V **dust trail:** is used to describe a number of dust particles in interplanetary space that have similar orbital parameters and originate from the same parent body. In contrast to the meteor streams dust trails do not necessarily cross the Earth’s orbit.
- W (meteorite) **fall**: a meteorite recovered on the ground that was observed during its entry such that its orbit can be determined.

When the words visual, photographic, telescopic, radio, photo-electric are combined with ‚meteor’ (A), they should indicate only the method of observation, since the dection limits of different techniques in the mass and in the velocity of entering meteoroids depend on several parameters. The approximate mass ranges are: radio meteors $m < 10^{-5}$ kg, optical meteors 10^{-8} kg $< m < 10^{-1}$ kg, fireballs: 10^{-1} kg $< m < 10^{3}$ kg, super bolides (fireballs typically observed from IR satellite networks) 10^{3} kg $< m < 10^{6}$ kg.

4.3.2.2 Observations

4.3.2.2.1 Optical observations

The meteor consists of a head and trail or train brightness. The meteor head is the brightness in the immediate surrounding of the meteoroid body that moves with the speed of the meteoroid and this is the brightest part. The train is the extended radiation observed behind the meteoroid body. Different types of trains are observed and arise from different physical processes. The most common optical meteor phenomena are listed in Table 1, those listed which are not discussed in detail here are described in [06Bor].

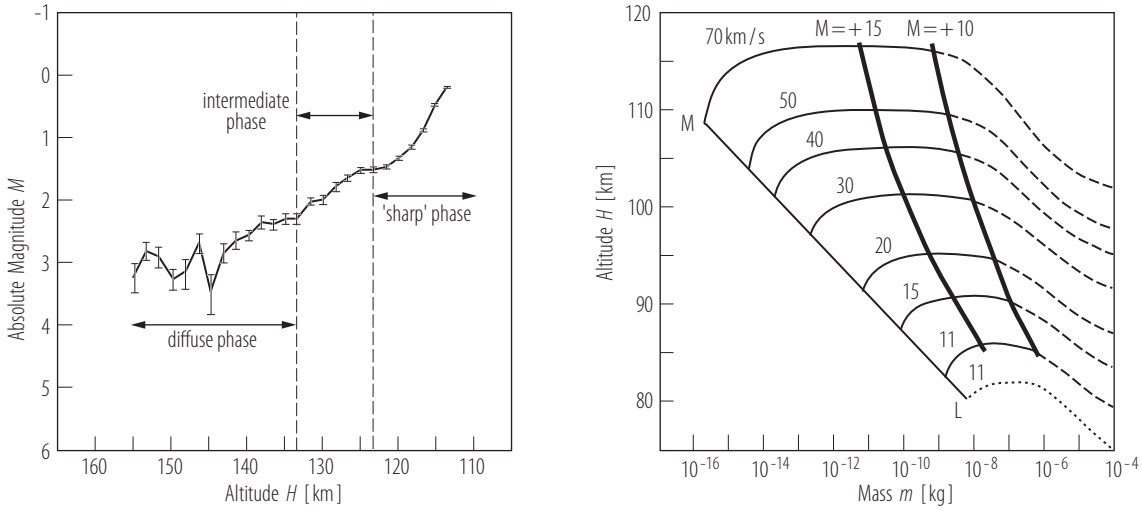

Fig. 1. (a) Optical light curve of the LN 98013 fireball showing an initial diffuse phase, an intermediate phase and the phase that corresponds to the classical ablation denoted by the observers here as ‚sharp phase' (from [00Spu]). **(b)** The altitude at which classical ablation of a single stony meteoroid entering at 45° zenith angle arises calculated for different masses and entry speeds. The heights are shown as solid lines for entry speeds 11 to 70 km s^{-1} for June standard atmospheric conditions 45°N. The dotted line is for December standard atmospheric conditions. The left line connecting points M and L denotes the range of mass and speed for which particles survive entry. The dashed lines denote the range for which the calculations do not apply, since the meteor brightness commences at higher altitude as a result of fragmentation [75Haw]. The bold solid lines depict the parameters of particles that produce trails of maximum electron line density 10^{10} m^{-1} and 10^{12} m^{-1} (radio magnitudes +15 and +10), from [98Cep].

Optical meteors are quantified based on the astronomical magnitude scale for apparent magnitudes, seen from the observer:

$$\mathcal{M}_1 - \mathcal{M}_2 = 2.5 \log (I_2/I_1) \quad (1)$$

where $\mathcal{M}_1$ and $\mathcal{M}_2$ are the respective magnitudes of two meteors and I_1,I_2 their luminous fluxes, defined as the power of light perceived by the human eye.

The absolute optical meteor magnitude scale, M_V, is normalized to a zenith distance of 100 km from the observer. For a meteor radiation P (in watts) in the optical regime the meteor magnitude M_V is ([02Haw] refering to [61Kin]):

$$M_V = 6.8 - 2.5 \log (P). \quad (2)$$

The luminous power P of a meteor in the optical (400 to 700 nm) regime is approximately proportional to the instantaneous ablation rate dm/dt:

$$P = \tau_1 \, 1/2 \, \mathrm{d}m/\mathrm{d}t \, v_E^2, \quad (3)$$

where v_E is the geocentric entry speed. The luminous efficiency factor, τ_l describes the amount of the energy of motion that is transformed into energy of electromagnetic radiation in the optical regime. It depends on the entry velocity and meteoroid properties in a complex way and varies with the spectral interval of the observations considered [98Cep], [02Haw]. Note that equation (3) neglects the energy transformed into energy of deceleration.

Table 1. Description of visual meteor phenomena

Type	Mechanism(s)	Phenomenon	Main conditions of appearance
head	instantanious line emission of neutral/ionized meteoroid and atmospheric species surrounding the meteoroid	major meteor brightness that lasts for about a second	altitude between 120 and 80 km (20 km for fireballs)
gaseous wake	line emission of rarified non-equilibrium gas that follows the head	emission spectrum different from the head spectrum evolves 100s of meters to several kilometers behind the head	altitude above 55 km
particulate wake	individual meteor heads formed around fragments released from the meteoroid	emission spectrum similar to meteor head	mostly at low altitude
flare	sudden fragmentation or change of physical parameters	sudden increase of meteor brightness by more than one magnitude	mostly for high velocity meteors
green train	reactions among atmospheric species	OI[1] 557.7 nm (forbidden line in the atomic spectrum of neutral oxygen) emission occuring from 1 to 2 s after meteor disappearance	mostly for high velocity meteors; height profile different from that of the meteor
persistent train	atomic recombination and/or chemiluminescence of cooling rarified gas	visible for tens of minutes after meteor disappearance; consist of afterglow phase, recombination phase and continuum	bright fireballs 75 to 100 km altitude
reflection train	sunlight scattered at fragment dust particles generated by fireballs	bright spectral continuum and band emission of metal oxides that lasts for hours	form at any height; observed during daytime or twilight

[1] Following convention in atomic spectroscopy "I" denotes the neutral atom, "II" the singly ionized atom, and so forth.

The visible light curve, i.e. the brightness as function of time is often sufficiently described by classical ablation theory. This considers heating and evaporation of the meteoroid material together with conservation of energy and momentum. Agreement with light curves improves when further adding a thermal fragmentation mechanism [04Pop, 04Cam]. Current ablation theories describe meteoroids that are small compared to the mean free path of surrounding atmospheric species ('free flow regime') as well as meteoroids that are large compared to the mean free path of surrounding atmospheric species. These latter ones generate an atmospheric shock, which changes the energy balance ('continuum flow regime'). The intermediate range ('transition regime' or 'slip flow regime') that can extend over heights of approximately 20 km is not fully described with analytical models [04Cam].

The light curves measured for specific atomic lines are different for different atomic species indicating differential ablation, i.e. the early ablation of volatile elements and only partial ablation of refractory elements [09Abe]. Meteor brightness is also observed above the altitudes for which classical ablation theory ('thermal ablation') predicts ablation (see Figure 1). The ablation at higher altitude is for instance caused by impacting atmospheric particles sputtering meteoroid material and/or by reactions of the atmospheric particles on the meteoroid surface.

Meteor spectra reveal line emission of the major meteoroid material and atmospheric species observed primarily as neutral atoms and singly charged atomic ions, as well as some molecular species. Head and gaseous wake brightness cover the same atomic emission lines, but with different abundance. There is currently no consistent physical model to describe the meteor phenomenon and the real process is far from thermodynamical equilibrium. Nevertheless, observed spectra are usually described with two gas components that are in thermal equilibrium with temperature ~5000 K for the main component and ~10 000 K for the second component. This model matches with most observed spectra and the emission lines of the main component are used to derive the chemical composition of meteoroids [93Bor] [00Bor] (see 4.3.2.4.3 below). The model fails, however, to describe high-resolution spectra [07Kas].

4.3.2.2.2 Radio observations

Radio waves are scattered by the electrons that are liberated along the path of the meteoroid generating the meteor trails and heads. The meteor trail or train can extend for meters to kilometers behind the meteoroid and trail echo durations range from tenths of seconds to minutes. The head echo typically lasts for less than tens of milliseconds and it originates from the plasma immediately surrounding the meteoroid. The meteor trail echoes dominate measurements by specular meteor radars (SMR) employing low power and small aperture radars such as AMOR and CMOR (and these are the conventional meteor radars). The meteor head echoes dominate measurements of high power, large aperture radars (HPLA), such as ALTAIR, Arecibo, and EISCAT. [08Pel]

Meteor trails are usually observed by SMRs as specular trails that occur when the radar beam is perpendicular the meteoroid path. This gives the maximum possible radar signal and this specific geometry usually occurs during observations along the paths of the meteors. HPLA radar observing close to perpendicular to the geomagnetic field lines can occasionally observe non-specular trails just after the head echo as shown seen in Fig. 2a (note, this is not a typical radio meteor trail signal).

To describe the radar signal observers distinguish between over-dense and under-dense trails and these form distinctly different shapes of echoes. In the case of high electron densities the plasma frequency exceeds the radar frequency and the meteor trail forms a totally reflecting obstacle to the radar signal. This case is denoted as over-dense trail. In the case of an under-dense meteor trail the plasma frequency is below the radar frequency. The waves penetrate the trail and are scattered at individual electrons, as well as interferences influence the signal. The over-dense echo power is rather constant until the expanding trail reaches the under-dense condition. After that the echo power falls exponentially as it does for the initially under-dense trails. Although depending on the radar frequency an approximate value that is often given for under-dense trails (for the case of the conventional meteor radars that have a small range of fequencies) is that the column electron density along the beam is $< 10^{14}$ m^{-1} [98Cep], [02Bag]. The reflective properties of the meteor trail and the surrounding atmosphere for a given radio frequency also limit the height of observations (radio ceiling effect) and a large fraction of the material from meteoroids $< 10^{-5}$ kg is released into the atmosphere, for instance, above the altitudes that are measured with SMRs [87Ols].

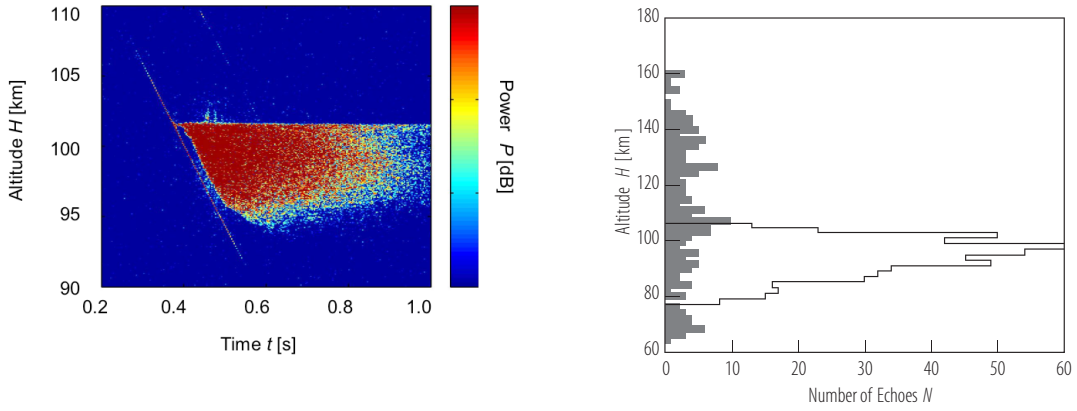

Fig. 2. (a) (see also color-picture part, page 626) The intensity of a meteor radar signal as function of time and altitude measured with the ALTAIR VHF radar (160 MHz) [07Clo]. The diagonal line at the left is the head echo signal, while the signal on the right of this line that extends in altitude and time is the non-specular trail signal. **(b)** Altitude distributions of the meteor head echoes (open histogram) and trail echoes (filled histogram) recorded during the December 1990 and December 1991 observing periods with EISCAT [04Pel].

The number, q of electrons in units electrons m^{-1} produced per distance along the path of the meteoroid is:

$$q = -\beta/\mu v \cdot \mathrm{d}m/\mathrm{d}t \tag{4}$$

with average mass, μ of ablated atoms, meteoroid speed, v, mass loss rate, $\mathrm{d}m/\mathrm{d}t$, and ionization coefficient, β. Approximate values of the ionization coefficient for $v > 35$ km s^{-1} are [83Bro]: $\beta = \beta_0 v^n$ with $\beta_0 = 3.02 \cdot 10^{-17}$, $n = 3.42$, and $[v]$ = m s^{-1}. Approximate values for $v > 35$ km s^{-1} are [97Jon] $\beta = 9.4 \cdot 10^{-6}(v\text{-}10)^2 v^{0.8}$ with $[v]$ = km s^{-1}. The empirically derived approximate relation to visual meteor magnitudes M_V is:

$$M_V = 36 - 2.5 (\log q - \log v) \tag{5}$$

with $[v]$ = km $s^{-1}$and $[q]$ = m^{-1} [61Kin]. Uncertainties arise in connecting the electron densities to magnitudes of visible meteors [63Kai],[02Bag].

Head echoes occur around meteoroids that enter the atmosphere at altitudes between about 80 and 120 km [04Pel], but typically in smaller range of altitudes than the trail echoes observed by HPLAs (see Fig.1.2.b). The time duration of most head echoes corresponds to the time it takes for the meteoroid to pass the radar beam, typically tens of milliseconds for the narrow HPLA beams and the speed of the headecho is identical to that of the entering meteoroid [08Wan]. Models to explain the meteor head echoes in terms of the atmospheric scattering process are still under debate [04Clo].

4.3.2.2.3 Data archives and information for observers

The Meteor Data Center of the International Astronomical Union (IAU) publishes a database of meteor observations [05Lin] on the homepage of the Astronomical Institute, Slovak Academy of Sciences. Further information including that about newly observed showers is available from the web site of the Poznan Observatory in Poland and this is also the contact for suggesting the dicovery of new meteor showers. The International Meteor Organization also provides information concerning observations of meteor orbits and fluxes on a web site.

4.3.2.3 Meteor fluxes, sources and orbits

4.3.2.3.1 Meteor fluxes and sources

As a result of the Earth's orbital motion and rotation meteor count rates are higher on the local dawn side and lower on the local dusk side (diurnal variations). Due to the tilt of the Earth's axis meteor flux variations depend on latitude. The largest differences in the amplitudes of the diurnal flux variations are seen at equatorial latitudes and they remain almost constant during the year. The diurnal variations seen at polar latitudes are smaller, but show the highest degree of seasonal variations [04Sza].

The flux of meteoroids into the atmosphere depends, among others, on their orbital parameters in interplanetary space. A straightforward calculation of absolute meteoroid fluxes and orbital distributions in interplanetary space from meteor observations is therefore not possible. Deriving absolute fluxes from meteor observations is further hampered by the complex dependence of the detection efficiencies and of the mass and velocity range of detectable meteoroids on the observation method and on the specific device. Moreover, the velocity of the meteoroid needs to be estimated and this has only high accuracy when derived from either interferometric or multi-static observations. The orbital information derived for the single meteor event in many cases has a low reliability, though orbital distributions are derived from meteor surveys and provide useful information (see Section 4.3.2.3.4).

The major meteoroids crossing Earth orbit originate from asteroids and comets. It is at present assumed that cometary meteoroids generate the majority of observed meteors, while asteroidal meteoroids generate the majority of the collected meteorites. This is supported by meteor properties that are derived from observations (see Section 4.3.2.4). Assuming the meteoroids are in bound orbit about the sun their maximum initial geocentric velocity v_g is 72 km s^{-1} corresponding to a meteoroid on parabolic orbit (heliocentric velocity $v_h \approx 42$ km s^{-1}) with inclination 180°, that is direction of motion opposite to the orbital motion of the Earth (velocity ≈ 30 km s^{-1}). Indeed most meteoroids reach the Earth with velocities below this value.

For a small fraction of meteors observers derive initial geocentric velocities that exceed 72 km s^{-1}. These meteoroids should in majority come from insterstellar space as was discussed by many observers in the past and is summarized in [98Cep]. Based on AMOR radar observations in New Zealand observers suggested that hyperbolic meteors originate from distinct source regions in the interstellar medium [96Tay]. The suggested origin of hyperbolic meteors from distinct interstellar source regions is not confirmed. Also other observers recently claimed the detection of interstellar meteors [00Sat, 05Jan]. The orbital parameters of the photographic meteor orbits from the Meteor Data Center show no convincing evidence for the detection of interstellar meteors and the number of observed hyperbolic orbits possibly results from the dispersion of the determined velocities [04Haw], [07Haj].

4.3.2.3.2 Meteoroid flux onto Earth

The uncertainties outlined above make it difficult to determine absolute meteoroid fluxes and especially to determine the flux onto Earth. Discussing the mass fluxes requires the distinction of the fluxes of meteoroids (1) crossing Earth orbit, (2) entering the Earth's atmosphere and (3) reaching the surface of the Earth. The mass flux may further vary in time. The flux of meteoroids crossing Earth orbit is derived from a variety of different observations including, aside from different types of meteor observations, in-situ measurements of dust from spacecraft, analyses of lunar crater and micro-crater statistics, as well as near-Earth asteroid observations (compiled by Ceplecha et al. [98Cep]). The derived cumulative mass distribution increases to the smaller sizes and is approximated with power laws of different exponents in different size intervals. The derived average flux over 100 years of meteoroids with masses < 10^8 kg is 2.4×10^7 kg yr^{-1} onto Earth and considering larger masses is not meaningful over this time interval [98Cep]. Derived from the same compilation the meteoroids with masses < 10^{-7} kg have an influx of 4×10^6 kg yr^{-1} onto Earth. A recent analysis of impact craters collected on an exposure experiment on a near-Earth satellite leads to significantly higher fluxes. Derived from these measurements carried out in the 1980s the total mass of dust in the size range 20 to 400 micrometer (approximate mass range 10^{-10} -

10^{-6} kg) that enters the Earth is 3×10^7 kg yr^{-1} [93Lov]. This is supported by an analysis of marine isotope records that suggests that the long term average accretion rate over the last 80 million years is 3.7 $\times 10^7$ kg yr^{-1} [96Peu]. While all these values are possibly influenced by experimental uncertainties the origin of the meteoroids from the fragmentation of asteroids, comets and other solar system objects make time variations very likely and all the results are within reasonable limits. It is estimated that out of the entering particles with size < 1 mm 90% vaporize during entry [98Tay]. The input of meteoroid material into the Earth's atmosphere is possibly highly variable in time. This is especially so, since the meteor showers, which have a minor contribution to the overall mass budget, are of considerable influence.

4.3.2.3.3 Meteor showers and their orbits

Meteor showers are groups of annually appearing meteors with a common radiant, i.e. the point at the sky from which a meteor shower seems to originate. The meteors related to the same shower are generated by meteoroids that were released from the same parent body and form a dust trail or a meteoroid stream in interplanetary space. Showers occur at the time during the year when the Earth orbit crosses the trail orbit, which is close, but not necessarily identical to the orbit of the parent body. The distribution of dust and meteoroids along the orbit is non-uniform and intensity of meteor showers varies from year to year. The apparent radiant undergoes a daily motion and for long lasting showers this can be significant. Strong showers are often called meteor storms.

A large number of meteor showers is proposed by observers and the IAU has established criteria for determining showers. Meteor showers are named after the current stellar constellation that contains the radiant. Greek letters of bright stars near the radiant or the month of appearance are used to distinguish multiple showers that seem to exhale from the same constellation. For showers whose maximum occurs during daytime hours the word ‚daytime' is added. For a detailed description see [08Jen].

Meteor shower activities are largely studied based on relations derived from visual observations, for which the human observer may induce uncertainties [02Haw]: The population index r, is the ratio of the numbers $N(\mathcal{M})$, $N(\mathcal{M}+1)$ of meteors of a magnitude $\mathcal{M}+1$ to the next brighter magnitude $\mathcal{M}$:

$$r = N(\mathcal{M}+1) / N(\mathcal{M}). \tag{6}$$

The Zenithal Hourly Rate *ZHR* is the calculated maximum number of meteors that an observer would see in perfectly clear skies with the shower radiant located at the observers zenith. Assuming a limiting visual magnitude of + *6.5* it is:

$$ZHR = F \cdot N/T_{eff} \cdot 1/\sin(e_R) \cdot r^{(6.5-\mathcal{M}_1)} \tag{7}$$

with a correction factor, *F,* describing the obstruction of the field of view of the observer, the number, N of meteors recorded during the time T_{eff} and $\mathcal{M}_1$ the limiting magnitude of the observation; e_R is the local elevation angle of the shower's radiant and this description is applicable for $e_R > 10°$. The hourly rate seen by one observer during a mean non-shower night is 10 [83All]. The mass distribution of meteors is described with the number, dN of meteors in the mass interval between m and m+dm with a power law:

$$dN = \text{const}\, m^{-s}\, dm \tag{8}$$

with s being the mass distribution index. If the shape of the meteor light curves does not significantly change among the considered observations s can be related to the population index r as:

$$s = 1 + 2.5 \log (r). \tag{9}$$

Table 2 lists the major meteor showers with their shower period (based on [98Cep]), *ZHR*, radiant, initial geocentric velocity v_g, and their maximum solar longitude. Further listed are the orbital parameters perihelion distance, q, semi-major axis, a (the two latter given in astronomical unit, AU), eccentricity, e, inclination, i, longitude of the perihelion, ω, and longitude of the ascending note Θ. A large number of showers exist and the table lists only showers with *ZHR* > 20 predicted for the year 2008 as published by the International Meteor Organization.

Table 2: Major meteor showers with *ZHR* > 20 predicted for 2008

Shower and period of activity	*ZHR*	Radiant α [°]	δ [°]	v_g [kms^{-1}]	λ_{sol} [°]	*q* [AU]	*a* [AU]	*e*	*I* [°]	ω [°]	Θ [°]
Quadrantids Jan1 - Jan5	120	231	49	41	283°16	0.98	3.0	0.66	72	170	283
η Aquarids Apr21 - May25	70+	338	–1	66	45°5	0.57	9.2	0.94	164	96	44
S δ Aquarids Jul12 - Aug19	20	339	–16	41	125°	0.09	2.7	0.97	25	149	310
Perseids Jul23 - Aug27	100	49	58	59	140°	0.95	24	0.96	113	150	139
Orionids Oct2 - Nov7	30	95	16	67	208°	0.58	17	0.97	164	81	28
Leonids Nov14 - 21	20+	153	22	71	235°27	0.98	15	0.93	162	172	235
Geminids Dec4 - 17	120	112	33	35	262°2	0.14	1.3	0.89	24	325	261

4.3.2.3.4 Sporadic meteors and their orbits

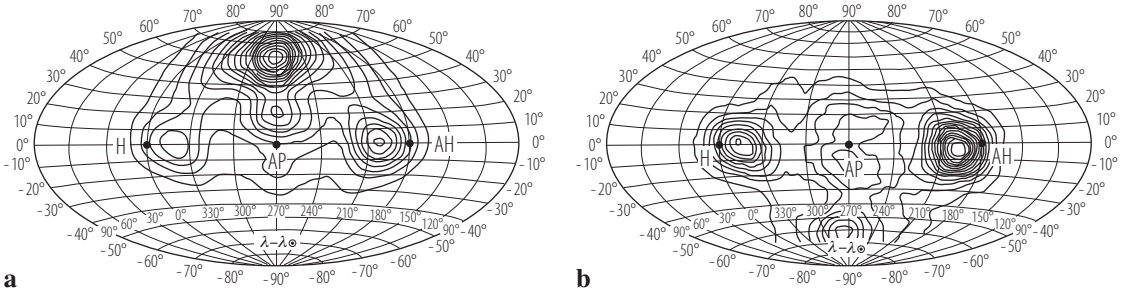

Fig. 3. (a) Contour plots of the distribution of meteor radiants in the Harvard radio surveys where H marks the position of the sun and AH the antihelion direction, AP is Earth's apex. **(b)** Contour plots of the distribution of meteor radiants in the Adelaide radio surveys. Both figures are based on an analysis [94Jon] of surveys compiled by the IAU Meteor Data Center, (figures from [98Cep]).

The majority of observed meteors are not associated with a shower and those meteors are called sporadic meteors. The fluxes of the observed sporadic radio meteors are empirically attributed to specific source regions (Table 3), but meteor flux rates vary with the observing location and specific radar facility (Fig. 3 a&b). The relative strength of the sources also varies with magnitude of radio meteors considered [94Jon]. The velocity distributions of the sporadic optical meteors are shown in Figures 4 a&b, their reciprocal semi-major axes in Figures 4 c&d. Note, that derived distributions of orbital parameters of sporadic meteors are not identical with the distribution of orbital parameters of meteoroids in interplanetary space (see Section 4.3.2.3.1.).

Table 3. Major sources in the radiant distribution of sporadic radiometeors [94Jon]:

Flux	longitude λ-λ_ψ	latitude β	width at half maximum Δ
North Apex	271°	19°	21°
South Apex	273°	–11°	not determined
Helion	342°	1°	16°
Antihelion	198°	0°	18°
North Toroidal	271°	58°	19°
South Toroidal	274°	–60°	16°

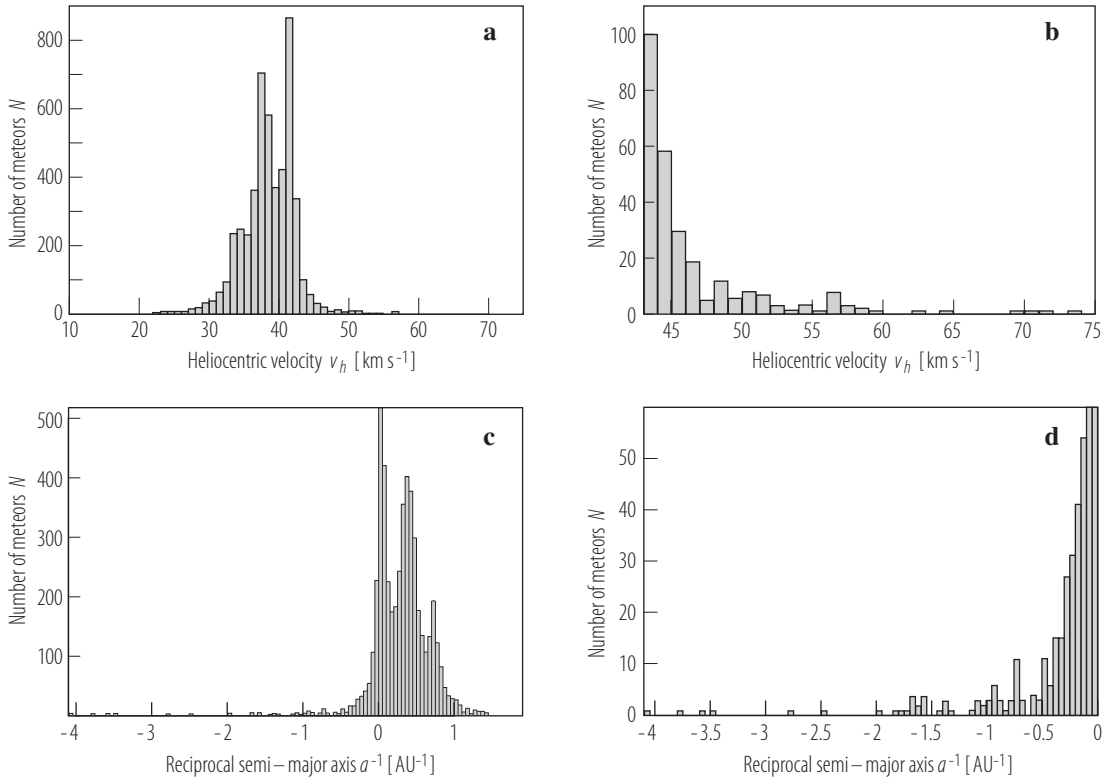

Fig. 4. (a) The distributions of derived heliocentric velocities of meteors in the IAU MDC photographic database over the entire interval of heliocentric velocity. **(b)** The same distribution for the interval of large heliocentric velocities. **(c)** The distributions of reciprocal semi-majoraxis derived from the IAU MDC photographic database. **(d)** Expanded plot of the sample of hyperbolic orbits (figures from [05Lin]).

4.3.2.4 Composition and properties

4.3.2.4.1 Fireballs and falls

A rarely occuring chance of studying meteor composition is the laboratory analysis of a remnant meteorite whose orbital characteristics have been derived from the observation of the corresponding meteor (‚fall'). Listed in Table 4 are the cases of meteorite falls (see Section 4.3.2.1.2) that were observed since the 1950s. All falls were classified as chondritic meteorites (see different chapter of this issue). Two of the fireballs, Přibram and Neuschwanstein had, almost, identical orbits, but are classified as different chondritic types.

Table 4. Recovered meteorite falls.

Meteorite	Year of fall	Recovered mass [kg]	Meteorite type	a [AU]	e	i [°]	Ref.
Přibram	1959	5.8	H5	2.4	0.67	10.5	61Cep
Lost City	1970	17	H5	1.7	0.42	12.0	71McC
Innesfree	1977	4.58	L5	1.9	0.47	12.3	78Hal
Peekskill	1992	12.57	H6	1.5	0.41	5	94Bro
Tagish Lake	2000	5 - 10	C	2.1	0.57	1.4	02Bro
Morávka	2000	1.4	H5-6	1.85	0.47	32.2	03Bor
Neuschwanstein	2002	6.2	EL6	2.4	0.67	11.41	03Spur
Park Forest	2003	18	L5	2.53	0.68	3.2	04Bro
Villalbeto de la pena	2004	5	L6	2.3	0.63	0	05Llo 06Tri

4.3.2.4.2 Meteoroid properties derived from meteor characteristics

Several groups of meteoroid populations with characteristic meteoroid properties are recognized from photographic and video observations. They correspond to groups derived from fireball observations. The groups differ in meteor beginning heights indicating the ablation properties as well as in derived orbital elements. The percentage of the observed meteors that belongs to a certain group depends on the considered type of observation. The meteor observations cover different masses depending on the respective observation method, the smallest mass is given as $2\ 10^{-8}$ kg, the largest mass as 0.5 kg, the observed fireballs are in the mass range from 0.1 to 2×10^3 kg. Separation of the populations solely based on orbital elements is not possible. Table 5 lists from left to right column the group classifications for meteors and fireballs, the orbital distributions for both groups, the ablation coefficient, the derived bulk denisity of entering meteoroid material, and the suggested meteoroid properties and sources.

The entry process of the meteoroid can be described by a set of differential equations [98Cep], and by reproducing the meteor brightness along the trajectory one can derive the ablation ability of the meteoroid material. This holds for the case of a single non-fragmenting body as well as for continuous fragmentation of the meteoroid and is expressed in terms of the ablation coefficient σ. Whilst their derived values are model dependent the observed meteors show clearly distinct ablations coefficients. The listed data refers to values and derivation of the ablation coefficients by [88Cep, 98Cep]. Deriving the bulk density of the entering meteoroid is possible for meteors for which the mass loss rate was obtained, but this is based on a number of assumptions and even for meteors of the same showers a wide range of density values is derived [02 Bab, 02Bel].

The meteors comprise of the groups A, B, C and D. Aside from these groups the orbital elements of a single meteor with suggested asteroidal origin (‘aster') are given. The orbital elements derived from the observations typically extend over a large range. The average orbital eccentricities, e, and semi-major axes, a, are given. Depending on the observations the A group meteors comprise of 27% to 50% of all observed meteors, the B group meteors amount to 2 - 5%, C group meteors to 41 - 67% and D group

meteors to 3 - 10%. Fireballs comprise of four major groups (I, II, IIIA, IIIB) with different ablation abilities. Their contributions to the observed fireballs in the mass range from 0.1 to 2000 kg are 29% (group I), 33% (group II), 26% (group IIIA) and 9% (group IIIB). A separate population attributed to iron meteoroids contains 3% of observed fireballs. The C1 and C2 meteor groups include classical meteor showers with known comet parent bodies, the D fireball group includes the Draconid meteor shower. The C3 group for meteors was found in observations of faint meteors [84Haw] and then its presence was investigated among the data of brighter meteors and fireballs. The given C3 group for meteors and for fireballs result from subtracting a population of random inclination orbits from the populations C1 and IIIA, respectively. This group of short-period orbits with random inclination distribution is in majority observed for masses $< 10^{-6}$ kg. Accordingly the A group meteors can be divided into subgroups with the same distributions of orbital parameters as C1, C2, and C3 [84Haw]. Among the Group I fireballs are the Príbram, Lost City and Innisfree meteorite falls. Though similar populations are found for meteors and fireballs, their relative amount differs: the populations that correspond to regular cometary material make up between 41 and 67 % of the meteor observations (i.e.groups C1, C2, C3), but only 26 % of fireball observations (groups IIIA, IIIAi and C3). The group I populations that makes up 29% of observed fireballs, corresponds to the observation of the single ‘asteroidal’ meteor.

4.3.2.4.3 Meteoroid compositions derived from meteor spectroscopy

The observed meteor brightness is produced by both meteoroid and atmospheric constituents, but the abundances of heavy elements that are derived from the observations are assumed to indicate the meteoroid composition. The abundances of the major elements contained in the entering meteoroids derived from fireball spectra [05Bor] are shown in Fig. 5a as the ratio of the elemental abundances $A' = A / A$ (Mg) to the element abundance in CI meteorites. The measurements are grouped according to the dynamic sources of the fireballs as Halley type comets, Jupiter family comets, asteroidal sources and fireballs associated with the Geminids. Shown for comparison are the element abundances of comet Halley dust derived from in-situ measurements during the Vega and Giotto flybys [88Jes] and those of LL ordinary chondrites [88Was].

Spectral classification of meteors based on the measured relative intensities of the Mg I, Na I, and Fe I emission lines are shown in a ternary diagram in Fig. 5b (from [05Bor]). Each symbol denotes one measurement of a meteor with the given classification. The points in the diagram are determined by the ratios of the observed line intensities Fe I/(Fe I+Mg I), Fe I/(Fe I+Na I), and Mg I/(Mg I+Na I) on a linear scale along the lines Fe I–Mg I, Fe I–Na I and Mg I–Na I, respectively. Normal meteors located in the middle part are called mainstream meteors classified as Fe - poor, Na- poor, and Na-enhanced meteors. Meteors that are not within the mainstream are classified as Fe-meteors, Na-free meteors, and Na-rich meteors. The solid line denotes the intensity ratio for meteors generated by particles with chondritic composition and entry speeds in km/s as indicated. The ratio is constant for speeds beyond 40 km/s [09Abe].

Table 5. Meteoroid populations derived from visual meteor and fireball observations [88Cep].

Observations						Suggested material & source		
Meteors		Fireballs	Orbital distribution			σ [s^2km^{-2}]	ρ [kg m^{-3}]	
Group		Group	a [AU]	e	i [°]			
---------		'iron'	ecliptic-concentrated small to moderate eccentricity			0.07	$7.8\ 10^3$	iron meteoroids asteroids
			1.8	0.5	6			
'ast.'		I	ecliptic-concentrated, moderate eccentricity			0.014	$2\ 10^3$	carbonaceous chondrites, comets, asteroids
			0.7 - 2.5	0.39 - 0.68	6 - 18			
A		II	ecliptic-concentrated, moderate eccentricity			0.42	$2\ 10^3$	carbonaceous chondrites, comets, asteroids
			1.6 - 2.5	0.55 - 0.64	1 - 14			
B		----------	ecliptic-concentrated, intermediate eccentricity, aphelia close to Jupiter			0.08	10^3	'dense' cometary material
			2.1 - 2.5	0.90 - 0.95	5 - 29			
C	C1	IIIA	ecliptic-concentrated, moderate eccentricity			0.10	750	cometary material, short period comets
			1.7 - 2.5	0.63 - 0.82	4 - 16			
	C2	IIIAi	random inclinations, high eccentricity			0.10		cometary material, long period comets
			-	0.99	random			
	C3	C3	random inclinations, moderate eccentricity			0.10		cometary material, (?) long period comets
			1.3 - 2.7	0.60 - 0.72	random			
D		IIIB	ecliptic-concentrated, moderate eccentricity			0.21	270	'soft' cometary material, short period comets
			2.6 - 3.3	0.66 - 0.77	13 - 25			

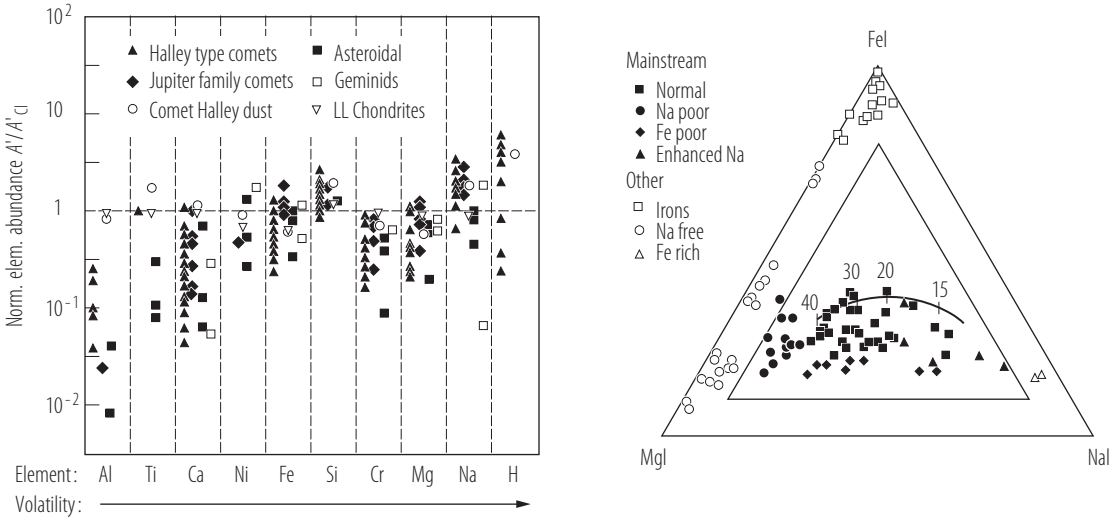

Fig. 5. (a) The element abundance of meteoroids derived from fireball spectra [05Bor] shown relative to that in CI meteorites and in comparison to cometary dust and LL ordinary chondrites. **(b)** Spectral classification of meteors (fainter than the fireballs) based on Mg I, Na I, and Fe I emission lines shown in ternary diagram with linear scale [05Bor], [09Abe].

4.3.2.5 References for 4.3.2

61Cep Ceplecha, Z.: Bull. Astron. Inst. Czech **12** (1961) 21-47.
61Kin McKinley, D. W. R.: "Meteor Science and Engineering", McGraw Hill, New York, 1961.
63Mil Millman, P.M.: Meteoritics **2** (1963) 7-11.
63Kai Kaiser, T. R.: Space Science Reviews **1(3)** (1963) 554-575.
71McC McCrosky, R.E., Posen, A., Schwartz, G., Shao, C.-Y: J. Geophysical Research **76** (1971) 4090-4108.
75Haw Hawkes, R. L., Jones, J.: Monthly Notices Roy. Astron. Soc. **173** (1975) 339-356.
78Hal Halliday, I. Blackwell, A.T., Griffin, A.A.: Journ. of the Royal Astronomical Society of Canada **72** (1978) 15-39.
80Hun Hunten, D.M., Turco, R.P., Toon, O.B.: Journal of the Atmospheric Sciences **37** (1980) 1342-1357.
83All Allen, C.W.: Astrophysical Quantities, 3rd ed., Athlone Press, London, reprinted 1983.
83Bro Bronshten, V. A.: Physics of Meteor Phenomena, D. Reidel, Dordrecht, The Netherlands, 1983.
94Bro Brown, P.G., Ceplecha, Z., Hawkes, R.L., Wetherill, G., Beech, M., Mossman, K.: Nature **367** (1994) 624-626.
84Haw Hawkes, R. L., Jones, J., Ceplecha, Z.: Bull. Astron. Inst. Czech. **35** (1984) 46 - 64.
87Ols Olsson-Steel, D., Elford, W.G.: Journal of Atmospheric and Terrestrial Physics **49** (1987) 243 - 258.
88Cep Ceplecha, Z.: Bull. Astron. Inst. Czechosl **39** (1988) 221-236.
88Jes Jessberger, E.K., Christoforidis, A., Kissel, J.: Nature **322** (1988) 691-695.
88Was Wasson, J.T., Kallemeyn, G.W.: Phil. Trans. R. Soc. London **A 325** (1988) 535-544.
93Bor Borovička, J.: Astron. Astrophys. **279** (1993) 627-645.
93Lov Love, S.G., Brownlee, D. E.: Science **262** (1993) 550-553.
93Ren Rendtel, J.: Handbook for Photographic Meteor Observations, Internatioal Meteor Organization, Antwerp, Belgium, 1993.
94Jon Jones, J., Brown, P.: Planetary and Space Science **42(2)** (1994) 123-126.
94Pel Pellinen-Wannberg, A., Wannberg, G.: J. Geophys. Res. **99** (1994) 11379-11390.
96Peu Peucker-Ehrenbrink, B.: Geochim, Cosmochim. Acta **60** (1996) 3187-3196.

96Tay Taylor, A.D., Baggaley, W. J., Steel, D.I.: Nature **380** (1996) 323-325.
97Jon Jones, W.: Monthly Notices Roy. Astron. Soc. **288** (1997) 995 - 1003.
98Cep Ceplecha, Z., J. Borovička, W.G., Elford, D. O. Revelle, R. L. Hawkes, Porubcan, V., Simek, M.: Space Sci. Rev. **85** (1998) 327-471.
98Tay Taylor, S., Lever, J.,H., Harvey, R.P.: Nature **392** (1998) 899-903.
99Zah von Zahn, U., Gerding, M., Höffner, J., McNeil, W. J., Murad, E.: Meteoritics & Planetary Science, **34(6)** (1999) 1017-1027.
00Bor Borovička, J., Jenniskens, P: Earth, Moon, and Planets **82/83** (2000) 399-428.
00Sat Sato, T. Nakamura, T., Nishimura, K.: IEICE Trans. Com. **E83-B (9)** (2000) 1990-1995.
00Spu Spurný, P., Betlem, H., Jobse, K., Koten, P., van't Leven, J.: Meteoritics and Planetary Science **35** (2000) 1109-1115.
01Nei McNeil, W.J., Dressler, R.A., Murad, E.: J. Geophys. Res. **106(A6)** (2001) 10447-10466
02Bab Babadzhanov, P.B.: Astron. Astrophys. **384** (2002) 317-321.
02Bag Baggaley, J.: in 02Mur.
02Bel Bellot Rubio, L.R., Marttınez Gonzalez, M.J., Ruiz Herrera, L., Licandro, J., Martiınez-Delgado, D., Rodrıguez-Gil, P., Serra-Ricart, M.: Astron. Astrophys. **389** (2002) 680-691.
02Bro Brown, P. ReVelle, D. Tagliaferri, E., Hildebrand, A.: Meteoritics and Planet. **37** (2002) 661-675.
02Clo Close, S., Oppenheim, M., Hunt, S., Dyrud, L.: J. Geophys. Res., **107(A10)** (2002) 1295, doi:10.1029/2002JA009253.
02Haw Hawkes, R.L.: in [02Mur], 2002.
02Mur Murad, E., I. P. Williams: "Meteors in the Earth's Atmosphere", Cambridge University Press, 2002.
02Wil Williams, I.P., Murad, E.: in [02Mur], 2002.
03Bor Borovička, J., Spurný, P., Kalenda, P., Tagliaferri, E.: Meteoritics Planet. **38** (2003) 975-987.
03Spur Spurný, P., Oberst, J., Heinlein, D., Nature **423** (2003) 151-153.
04Cam Campbell-Brown, M. D.; Koschny, D.: Astron. Astrophys. **418** (2004) 751-758.
04Bro Brown, P., Pack, D., Edwards, W.N., ReVelle, D., Yoo, B., Spalding, R., Tagliaferri, E.: Meteoritics Planet. Sci. **39** (2004) 1781-1796.
04Clo Close, S., Oppenheim, M., Hunt, S., Coster, A.: Icarus **168(1)** (2004) 43-52.
04Haw Hawkes, R.L., Mann, I., Brown, P.G.: Modern Meteor Science, 2004.
04Hil Hill, K.A., Rogers, L.A., Hawkes, R.L.: Earth, Moon, and Planets **95** (2004) 403-412.
04Pel Pellinen-Wannberg, A.: Atmos. Chem. Phys. **4** (2004) 649-655.
04Pop Popova, O.: Earth, Moon, and Planets **95(1-4)** (2004) 303-319.
04Sza Szasz ,C., Kero, J., Pellinen-Wannberg, A., Mathews, J.D., Mitchell, N.J., Singer, W.: Earth, Moon, and Planets **95** (2004) 101-107.
05Bor Borovička, J., Koten, P. Spurný, P, Bocek, J. Štork, R.: Icarus **174** (2005) 15-30.
05Jan Janches, D., Chau, J.L.: J. Atmospheric and Solar-Terrestrial Phys. **67** (2005) 1196-1210.
05Lin Lindblad, B.A., Nesluvan, L., Porubcan, V., Svore, J.: Earth, Moon, and Planets **93** (2005) 249-260.
05Llo Llorca, J., Trigo-Rodrguez, J.M., Ortiz, J.L., Docobo, J.A., Garcia-Guinea, J., Castro-Tirado, A.J., Rubin, A.E., Eugster, O., Edwards, W., Laubenstein, M., Casanova, I.: Meteoritics Planet. Sci. **40** (2005) 795-804.
06Bor Borovička, J., Roya. J.: Astron. Soc. Canada **100** (2006) 194-198.
06Tri Trigo-Rodrguez, J.M., Borovička, J., Spurný, P., Ortiz, J.L., Docobo, J.A., Castro-Tirado, A.J., Llorca, J.: Meteoritics Planet. Sci. **41** (2006) 505-517.
07Chr Christou, A.A., Oberst, J., Koschny, D., Vaubaillon, J., McAuliffe, J.P., Kolb, C., Lammer, H., Mangano, V., Khodachenko, M., Kazeminejad, B., Rucker, H. O.: Planetary and Space Science **55(14)** (2007) 2049-2062.
07Clo Close, S., Brown, P., Campbell-Brown, M., Oppenheim, M., Colestock, P.: Icarus **186**(2) (2007) 547-556.
07Haj Hajduková, M: Earth, Moon, and Planets, 10.1007/s11038-007-9171-5, 2007.
07Kas Kasuga, T., Iijima, T., Watanabe, J.: Astron. Astrophys. **474(**2) (2007) 639-645.

08Jen Jenniskens, P.: Earth Moon Planet (2008), doi: 10.1007/s11038-007-9155-5.
08Meg Megner, L., Siskind, D.E., Rapp, M., Gumbel, J.: J. Geophys. Res. **113** (2008), doi:10.1029/2007JD009054
08Pel Pellinen-Wannberg, A., Wannberg, G., Kero, J., Szasz, C., Westman, A.: Radio Science Bulletin. The Internatioal Union of Radio Science **324** (2008) 17-28.
08Wan Wannberg, G., Westman, A., Kero, J., Szasz, C., Pellinen-Wannberg, A.: The EISCAT meteor code, Ann. Geophys. **26** (2008) 2303-2309.
09Abe Abe, S., in: (I. Mann, A.M. Nakamura, T. Mukai Eds.) Small Bodies in Planetary Systems, Lecture Notes in Physics 758, Springer, Berlin Heidelberg, 2009.